$3 - D$ Geometry reconstruction using a color image stereo pair and partial differential equations

Luis Alvarez and Javier Sánchez
Departamento de Informática y Sistemas
Universidad de Las Palmas de G.C.
Campus Universitario de Tafira
35017, Las Palmas
Email: {lalvarez/jsanchez}@dis.ulpgc.es
WebPage: http://serdis.dis.ulpgc.es/~lalvarez/

Abstract

In this work, we present a new model for a dense disparity estimation and the $3 - D$ geometry reconstruction using a color image stereo pair. First, we present a brief introduction to the $3 - D$ Geometry of a camera system. Next, we propose a new model for the disparity estimation based on an energy functional. We look for the local minima of the energy using the associated Euler-Lagrange partial differential equation. This model is a generalization to color image of the model developed in [2], with some changes in the strategy to avoid the irrelevant local minima. We present some numerical experiences of $3 - D$ reconstruction, using this method for some real stereo pairs.

1 The $3 - D$ geometry of a camera system and the calibration problem.

This section is an introduction to the $3 - D$ geometry of a camera system and the calibration problem. Most of the results presented in this section can be found (with much more details) in [17]. To study the problem of camera calibration, we will use the classical "pinhole model" which assumes the simplest projective model for the camera image acquisition. The camera is represented by a projection plane $\mathcal{R}$ in $3 - D$ and a focus $C = (C_x, C_y, C_z)$. The projection of the point $M = (x, y, z)$ of the $3 - D$ scene into the camera is given by the interception of the line $\overline{MC}$ with the plane $\mathcal{R}$, (see figure 1).
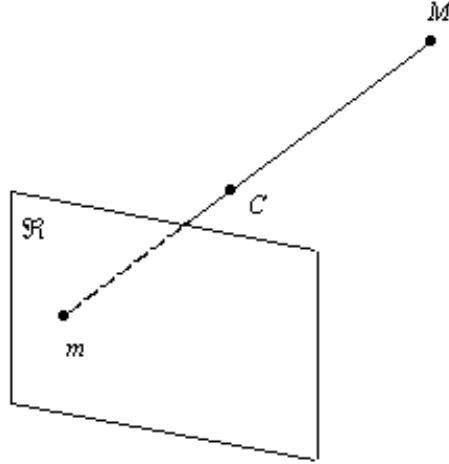
Figure 1: Projection of a 3-D point in the camera plane.

To calibrate the camera means to find out the parameters which determine the way that the projection works. There are 2 types of parameters: the intrinsic parameters and the extrinsic parameters. A digital color image $I(x,y) = (I_1(x,y), I_2(x,y), I_3(x,y))$ is given by 3 matrices where the values $I_k(x,y)$ $k = 1, 2, 3$ represent the 3 color channels (red, green and blue) in each pixel (x,y). The pixels represent small cells where the light arrive into the camera. The intrinsic parameters are the focal length f, the pixel size (p_x, p_y) and the position (c_x, c_y) into the camera of the interception point between the plane $\mathcal{R}$ and the perpendicular line to $\mathcal{R}$ passing through the focus C. For instance, if the focus is centered with respect to the plane image dimension then:

$$c_x = \frac{Number\ of\ horizontal\ pixels}{2}$$
$$c_y = \frac{Number\ of\ vertical\ pixels}{2}$$

from a projective point of view f and (p_x, p_y) are not independent in the sense that if we take a constant k the projection generated by the intrinsic parameters f and (p_x, p_y) is the same that the one generated by the parameters kf and (kp_x, kp_y). Then, instead of using the parameters f and (p_x, p_y), we use the normalized parameters $\alpha_x = p_x/f$ and $\alpha_y = p_y/f$. So to conclude, we have 4 intrinsic parameters: $\alpha_x, \alpha_y, c_x, c_y$. The intrinsic parameters do not depend on the camera location in the $3 - D$ scene. In figure 2 we illustrate the intrinsic parameters.

The extrinsic parameters of the camera determine the $3 - D$ location of the camera in the scene with respect to some "a priori" fixed reference system. The extrinsic parameters are given by a translation vector $t = (t_x, t_y, t_z)$ and a rotation matrix $R = (r_{ij})$ with respect to the fixed reference system. Since a rotation is given by 3 parameters (the rotation axe
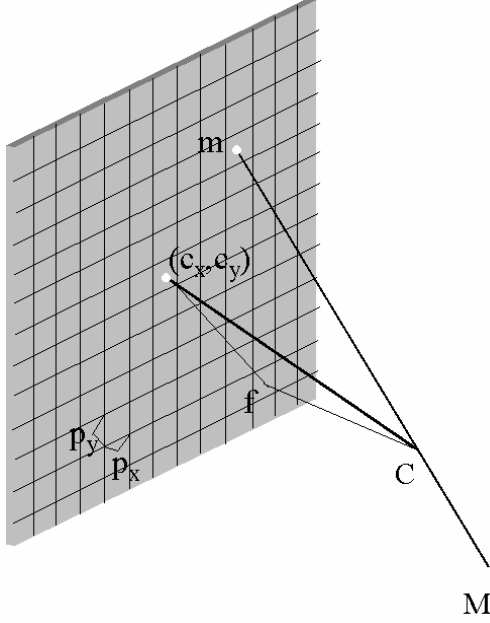
Figure 2: Intrinsic parameters illustration

and the rotation angle), therefore, they are 6 extrinsic parameters. In figure 3 we illustrate the extrinsic parameters

The next result establish how the intrinsic and extrinsic parameters determine the way the projection works.

Theorem 1 *(Faugeras [17]) Let be $\widetilde{M} = (M_1, M_2, M_3, M_4) \in \mathcal{P}^3$, then the projection point $\widetilde{m} = (m_1, m_2, m_3) \in \mathcal{P}^2$ of a $3-D$ point $\widetilde{M}$ in the camera is given by*

$$\begin{pmatrix} m_1 \\ m_2 \\ m_3 \end{pmatrix} = \begin{pmatrix} \alpha_x \mathbf{r}_1 + c_x \mathbf{r}_3 & \alpha_x t_x + c_x t_z \\ \alpha_y \mathbf{r}_2 + c_y \mathbf{r}_3 & \alpha_y t_y + c_y t_z \\ \mathbf{r}_3 & t_z \end{pmatrix} \begin{pmatrix} M_1 \\ M_2 \\ M_3 \\ M_4 \end{pmatrix} \tag{1}$$

where $\mathbf{r}_i$ represents the rows of the rotation matrix R. In what follows, we note by P the $4x3$ matrix which determines the projection, that is $\widetilde{m} = P\widetilde{M}$. We note that the matrix P is a linear projective application which is defined up to a scale factor.

To calibrate the camera we will assume that we know a set of $3-D$ points $\widetilde{M_i}$ and their respective projections $\widetilde{m_i}$ in the camera. So we formulate the calibration problem as to find out a P matrix such that:

$$\widetilde{m_i} = P\widetilde{M_i} \qquad \forall i = 1, .., N \tag{2}$$
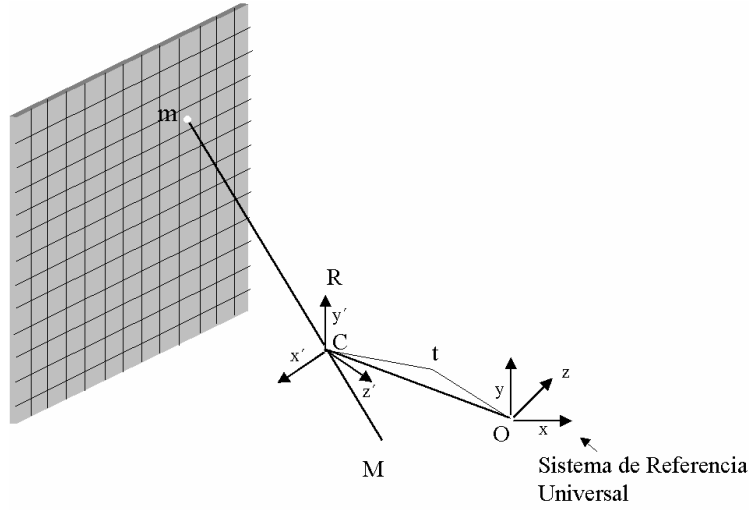
3

Figure 3: Extrinsic parameters illustration

where N is the number of points that we use. In practice, we will use a special object shown in figure 4 for which we know the $3 - D$ position of the black squares. In fact we will use as points $\widetilde{M_i}$ the corners of the black squares, and as points $\widetilde{m_i}$ the projection of $\widetilde{M_i}$ into the camera.

We note that matrix P has 12 elements, and that for each $(\widetilde{M_i}, \widetilde{m_i})$ equation (2) provides (once the projective parameter is removed), 2 linear equations with respect to P elements given by:

$$\sum_{i=1}^{3} p_{1i} M_i + p_{14} - m_1 \left(\sum_{i=1}^{3} p_{3i} M_i + p_{34} \right) = 0 \qquad (3)$$

$$\sum_{i=1}^{3} p_{2i} M_i + p_{14} - m_2 \left(\sum_{i=1}^{3} p_{3i} M_i + p_{34} \right) = 0$$

When N (the number of pairs $(\widetilde{M_i}, \widetilde{m_i})$) is bigger than 5, and the points are in general position (that is, they are not in some special degenerated configuration) then, we can recover matrix P following the relation (2). The technique to estimate P is very simple. We note by $p = (p_{11}, p_{12,....}, p_{34})$ the 12 elements vector given by the lines of matrix P. Then, the relations (3) can be written as $Ap = 0$, where A is a $2Nx12$. matrix. Since p is defined up to a scale factor, we can assume that $\|p\| = 1$. Then, we look for a vector p which minimize the energy $E(p)$ given by:

$$E(p) = \|Ap\|^2 = p^T A^T Ap$$

with the constraint $\|p\| = 1$. A straightforward computation yields to p equal to the eigenvector associated to the smallest eigenvalue of $A^T A$. On the other hand, using stan-
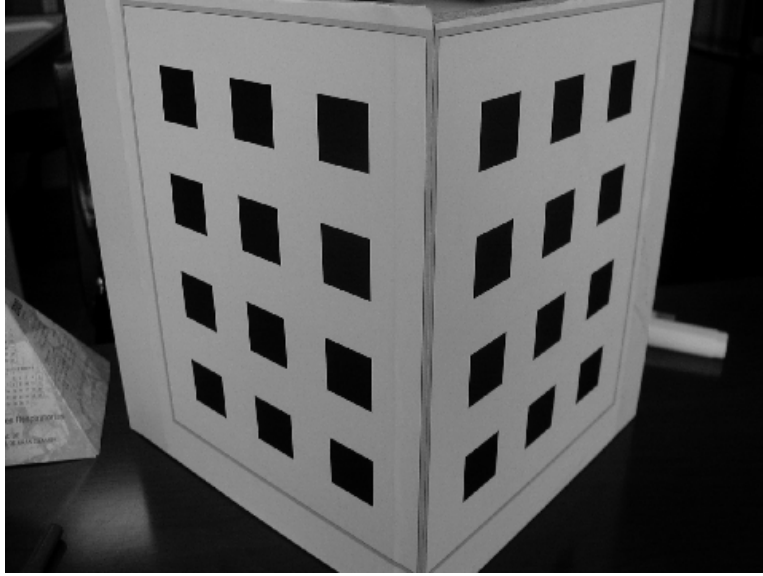
4

Figure 4: $3 - D$ object used for camera calibration

dard techniques, once the matrix P is known, we can deduce the intrinsic and extrinsic parameters.

Even if matrix P is a projective application and it is defined up to a scale factor, we can recover some very useful euclidean information from P. First, we can recover the focus position C of the camera:

$$C = -\widehat{P}^{-1} \begin{pmatrix} p_{14} \\ p_{24} \\ p_{34} \end{pmatrix}$$

and given a point $m = (m_1, m_2)$ in the camera, the director vector $\overrightarrow{mC}$ of the line $\overline{mC}$ is given by:

$$\overrightarrow{mC} = \widehat{P}^{-1} \begin{pmatrix} m_1 \\ m_2 \\ 1 \end{pmatrix}$$

where

$$\widehat{P} = \begin{pmatrix} p_{11} & p_{12} & p_{13} \\ p_{21} & p_{22} & p_{23} \\ p_{31} & p_{32} & p_{33} \end{pmatrix}$$

Then, using P, we can associate the line $\overline{mC}$ to any point m in the camera where the $3 - D$ point M has to be located.

The Epipolar Geometry

Until now, we have focused our attention in the case of 1 camera. In the case of 2 cameras, we have two views of the same scene. Each camera has its own matrix P that we will note by P and P' and for any $3 - D$ point M, there exist two projections m and m'. We note that if we know P and P' and two corresponding points m and m', then, we can recover the $3 - D$ position of M as the interception of lines $\overline{mC}$ and $\overline{m'C'}$. This is illustrated in figure 5.
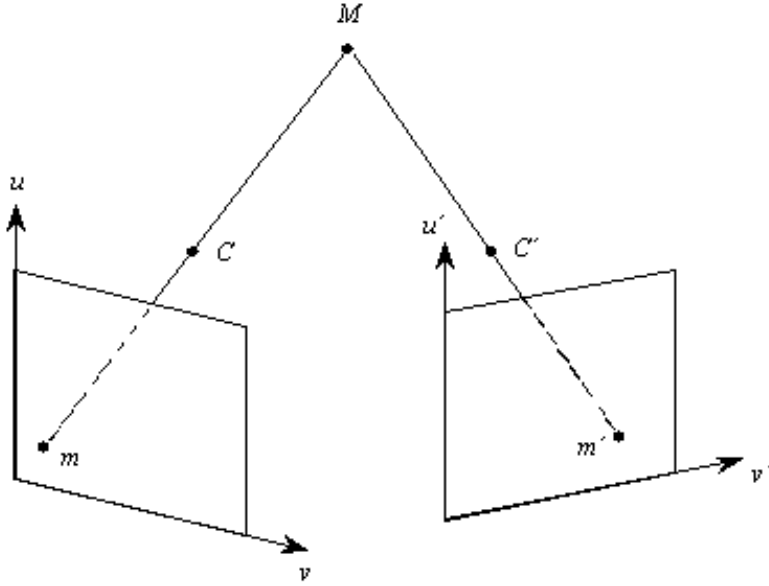

Figure 5: $3 - D$ Geometry of a stereo pair.

The point m' that corresponds to m in the other camera has to lie in the projection of the line $\overline{mC}$ in the other camera. This projection is named epipolar line associated to m. A straightforward calculus yields to the following expression for the epipolar lines:

$$(m'_1, m'_2, 1) \left(\left[P'\widetilde{C} \right]_x P'\widehat{P}^{-1} \right) \begin{pmatrix} m_1 \\ m_2 \\ 1 \end{pmatrix} = 0$$

where the symbol $[\, t\,]_x$ associated to a vector t is the antisymmetric matrix:

$$[\, t\,]_x = \begin{pmatrix} 0 & -t_z & t_y \\ t_z & 0 & -t_x \\ -t_y & t_x & 0 \end{pmatrix}$$

the $3x3$ matrix $F = \left[P'\widetilde{C} \right]_x P'\widehat{P}^{-1}$ is named fundamental matrix, and it determines the epipolar geometry, that is, it determines the epipolar line associated to each point m. In
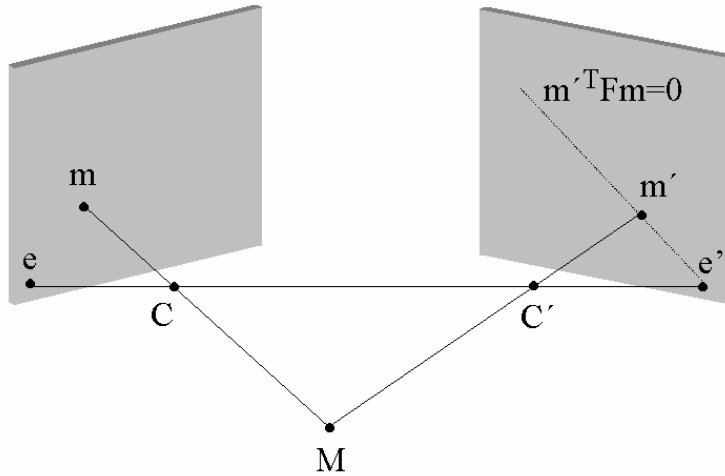
Figure 6: Epipolar Geometry

figure 6 we illustrate the epipolar geometry. The epipoles are the interception of the line $\overline{CC'}$ with the planes in both cameras.

2 Dense disparity map estimation and partial differential equations.

We name disparity to the displacement between the point m on the image I and its corresponding point m' on I'. The accuracy of the disparity estimation is very important because it determines the quality of the $3 - D$ reconstruction

Over the years, numerous algorithms for stereo vision have been proposed, which use different strategies.

- **Feature based:** Those algorithms establish correspondences between some selected features extracted from the images [23], such as edge pixels [41, 43], line segments [6, 31, 32] or curves [12, 39, 47]. Their main advantage is to yield accurate information and to manipulate reasonably small amounts of data, thus gaining in time and space complexity. Their main drawback is the sparseness of the recovered depth information. This class of methods has been widely used some years ago, when it was not possible to retrieve a dense and accurate reconstruction within a reasonable amount of time.

7

- **Area based:** In these approaches, dense depth maps are provided by correlating the grey levels of image patches in the views being considered, assuming that they present some similarity [15, 18, 22, 40]. These methods are well adapted for relatively textured areas; however, they generally assume that the observed scene is locally front-parallel, which causes problems for slanted surfaces and in particular near the occluding contours of the objects. Lastly, the matching process does not take into account the edge information which is actually a very important information that should be used in order to get reliable and accurate dense maps.

- **Energy based:** A last kind of approach which does not suffer any of the short-comings presented above, consists of solving the correspondence problem in a minimization and regularization formulation [2, 7, 9, 25, 45, 46, 49, 56].

The method that we propose in this paper belong to the energy based methods. To establish the model we will introduce some notations: we note by $F = (f_{ij})$ the fundamental matrix associated to the stereo pair. We define the auxiliary functions: $a(x, y), b(x, y)$ and $c(x, y)$ in the following way:

$$
\begin{aligned}
a(x, y) &= f_{11}x + f_{12}y + f_{13}, \\
b(x, y) &= f_{21}x + f_{22}y + f_{23}, \\
c(x, y) &= f_{31}x + f_{32}y + f_{33}.
\end{aligned}
$$

with this notation, the epipolar line associated to a point $m = (x, y)$ is given by:

$$a(x, y)x' + b(x, y)y' + c(x, y) = 0. \tag{4}$$

we will use this equation in order to parametrize the displacement between a point $m = (x, y)$ on I and its corresponding point $m' = (x', y')$ on I'.

2.1 Parametrization of the disparity

Under the assumption that corresponding points in both images have equal color levels, to estimate the disparity is equivalent to look for a vector function $\overrightarrow{h}(x, y) := (u(x, y), v(x, y))^t$ such that:

$$I_i(x, y) = I_i'(x + u(x, y), y + v(x, y)) \qquad \forall (x, y) \in \mathbb{R}^2. \qquad i = 1, 2, 3 \tag{5}$$

where I_i (respect. I_i') represent the 3 color channels of image I (respect. I'). We note that the corresponding point $(x', y') = (x + u(x, y), y + v(x, y))$ belongs to the epipolar line associated to (x, y) and then it satisfies:

$$R_e(x', y') = a(x, y)(x + u(x, y)) + b(x, y)(y + v(x, y)) + c(x, y) = 0$$

8

If we parametrize the epipolar line using a function $\lambda(x,y)$ then we obtain:

$$u(x,y) = \frac{-\lambda(x,y)b(x,y)}{\sqrt{a^2(x,y) + b^2(x,y)}} - \frac{a(x,y)x + b(x,y)y + c(x,y)}{a^2(x,y) + b^2(x,y)}a(x,y),$$

$$v(x,y) = \frac{\lambda(x,y)a(x,y)}{\sqrt{a^2(x,y) + b^2(x,y)}} - \frac{a(x,y)x + b(x,y)y + c(x,y)}{a^2(x,y) + b^2(x,y)}b(x,y),$$

where $\lambda(x,y)$ represents the parameter of the epipolar line. We will note $\overrightarrow{h}(\lambda(x,y)) = (u(\lambda(x,y)), v(\lambda(x,y)))$ to indicate that the disparity term depends just on the parameter $\lambda(x,y)$. We point out that the case $\lambda(x,y) = 0$ determines the point in the epipolar line which minimize the distance between the epipolar line and $m = (x,y)$. In figure 7 we illustrate the disparity parametrization using $\lambda(x,y)$.
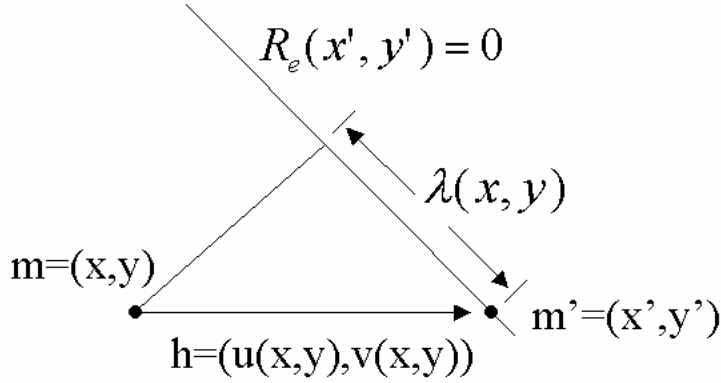
Figure 7: Parametrization of the disparity

Next, we present the model that we propose to estimate $\lambda(x,y)$.

2.2 The proposed energy model

To estimate $\lambda(x,y)$, we will consider the next energy functional:

$$
\begin{aligned}
E(\lambda) &= \sum_{i=1}^{3} \int_{\Omega} \left(I_i(x,y) - I_i'(x + u(\lambda(x,y)), y + v(\lambda(x,y)))\right)^2 \, dx\,dy \\
&+ C \int_{\Omega} (\nabla\lambda)^T D(\nabla I_{\max}) \nabla\lambda \, dx\,dy
\end{aligned}
\tag{6}
$$

9

where Ω is the image domain, C is a positive constant $I = (I_1, I_2, I_3)$ (respect. $I' = (I'_1, I'_2, I'_3)$) represent the color images of the stereo pair. $D(\nabla I_{\max})$ is the matrix given by:

$$D(\nabla I_{\max}) = \frac{1}{|\nabla I_{\max}|^2 + 2\nu^2} \left\{ \begin{bmatrix} \frac{\partial I_{\max}}{\partial y} \\ -\frac{\partial I_{\max}}{\partial x} \end{bmatrix} \begin{bmatrix} \frac{\partial I_{\max}}{\partial y} \\ -\frac{\partial I_{\max}}{\partial x} \end{bmatrix}^t + \nu^2 Id \right\}$$

where Id denotes the identity matrix and

$$\nabla I_{\max}(x,y) = \{ \nabla I_{i_0}(x,y) \ such \ that \ \|\nabla I_{i_0}(x,y)\| \geq \|\nabla I_i(x,y)\| \quad \forall i = 1,2,3 \}$$

Basically, the above energy functional establish a balance between the equality of the color channels between the corresponding points and the regularity of the function $\lambda(x,y)$. We can interpret the regularity term in the following way:

$$(\nabla \lambda)^T D(\nabla I_{\max}) \nabla \lambda \simeq \left\{ \begin{array}{l} \|\nabla \lambda(x,y)\|^2 \ if \ \|\nabla I_{\max}(x,y)\| \simeq 0 \\ \left(\frac{\partial \lambda}{\partial \nabla I_{\max}^{\perp}} \right)^2 \ if \ \|\nabla I_{\max}(x,y)\| >> 0 \end{array} \right.$$

This regularity term is an extension,in the case of color images, of the one proposed in [34, 36] developed in the context of optic flow estimations in an image sequence. This method has demonstrated its performance numerous times in the context of optical flow estimations [3, 4, 8, 16, 34, 35, 36, 50].

The energy model presented in this paper is a generalization, in the case of color images, to the one proposed in [2], with some changes in the strategy to avoid the irrelevant local minima. In [2] authors use a focusing strategy based on a linear gaussian multiscale analysis in order to avoid the irrelevant local minima. In this work we propose a pyramidal strategy which speed up the algorithm. We compute the disparity in a small version of the original images and then we extrapolate the information toward the original stereo pair. On the other hand, in this paper, we build our own calibration system in order to perform the numerical experiences.

2.3   Energy minimization.

In order to compute the minima of the energy functional, we are going to use the associated Euler-Lagrange partial differential equation. This Euler-Lagrange equation is given by:

$$C \operatorname{div}\left(D(\nabla I_{\max}) \nabla \lambda \right) + \sum_{i=1}^{3} \left(I_i(\overrightarrow{x}) - (I'_i)^{\lambda}(\overrightarrow{x}) \right) \frac{a \left(\frac{\partial I'_i}{\partial y} \right)^{\lambda}(\overrightarrow{x}) - b \left(\frac{\partial I'_i}{\partial x} \right)^{\lambda}(\overrightarrow{x})}{\sqrt{a^2 + b^2}} = 0, \tag{7}$$

where $\vec{x} = (x, y)$, and the superscript λ indicates a displacements of magnitude $(u(\lambda(x,y)), v(\lambda(x,y)))$, that is, for instance $(I'_i)^{\lambda}(\vec{x}) = I'_i(\vec{x} + (u(\lambda(x,y)), v(\lambda(x,y))))$. In the interior of the homogeneous part of the image I, $|\nabla I_{\max}| \to 0$, and then the eigenvalues λ_1 and λ_2 of matrix $D(\nabla I_{\max})$ behave as $\lambda_1 \to 1/2$ and $\lambda_2 \to 1/2$. In the case of a point in the edges of image I, $|\nabla I_{\max}| \to \infty$, and then $\lambda_1 \to 0$ and $\lambda_2 \to 1$. This behavior of the eigenvalues shows the anisotropic character of the regularization term.

In general, the Euler–Lagrange equation (7) will have multiple solutions. Typically, we may expect that the algorithm converges to a local minimum of the energy functional (6) that is located in the vicinity of the initial data. To avoid convergence to irrelevant local minima, we will use a pyramidal strategy to compute the disparity. That is, from the original stereo pair I and I', we define the pyramid of images I^{2^n}, I'^{2^n} where $n = 0$ corresponds to the original images, and I^{2^n}, I'^{2^n} is defined in the following recursive way: In order to go from image $I^{2^{n-1}}$ to image I^{2^n} we apply a linear smoothness filter to $I^{2^{n-1}}$ and then we perform a sampling of the image, in such a way that we keep 1 pixel from each 4 pixels. We perform this procedure a number of times that we note by n_0.

Next, we compute the disparity in the step n_0 by applying a gradient descent method to the Euler-Lagrange equation. We use as initial guest for the method the disparity computed using some simple technique as for instance a correlation window technique. We note that in the step n_0 the images are quite small, so the disparity estimation is much simpler and we reduce the risk to be trapped in irrelevant local minima.

Once the disparity in the step n_0 is computed, we extrapolate the value of the disparity to the step $n_0 - 1$. In order to do that, we use again the gradient descent method in the step $n_0 - 1$, but using as initial guest an extrapolation of the disparity previously computed in the step n_0. We point out that if the displacement, in the step n_0, between 2 points in both images is given by $(u(x,y), v(x,y))$, then, the displacement in the step $n_0 - 1$ is given by $(2u(2x, 2y), 2v(2x, 2y))$. In this way we compute the disparity in all the steps until the original stereo pair is reached.

We note that when we modify the image size, we have to take into account that the epipolar geometry changes. In fact, we can show easily that if we note by $F^{2^n} = \left(f_{ij}^{2^n}\right)$ the fundamental matrix in the step n, then:

$$\begin{pmatrix} f_{11}^{2^n} & f_{12}^{2^n} & f_{13}^{2^n} \\ f_{21}^{2^n} & f_{22}^{2^n} & f_{23}^{2^n} \\ f_{31}^{2^n} & f_{32}^{2^n} & f_{33}^{2^n} \end{pmatrix} = \begin{pmatrix} 4f_{11}^{2^{n-1}} & 4f_{12}^{2^{n-1}} & 2f_{13}^{2^{n-1}} \\ 4f_{21}^{2^{n-1}} & 4f_{22}^{2^{n-1}} & 2f_{23}^{2^{n-1}} \\ 2f_{31}^{2^{n-1}} & 2f_{32}^{2^{n-1}} & f_{33}^{2^{n-1}} \end{pmatrix}$$

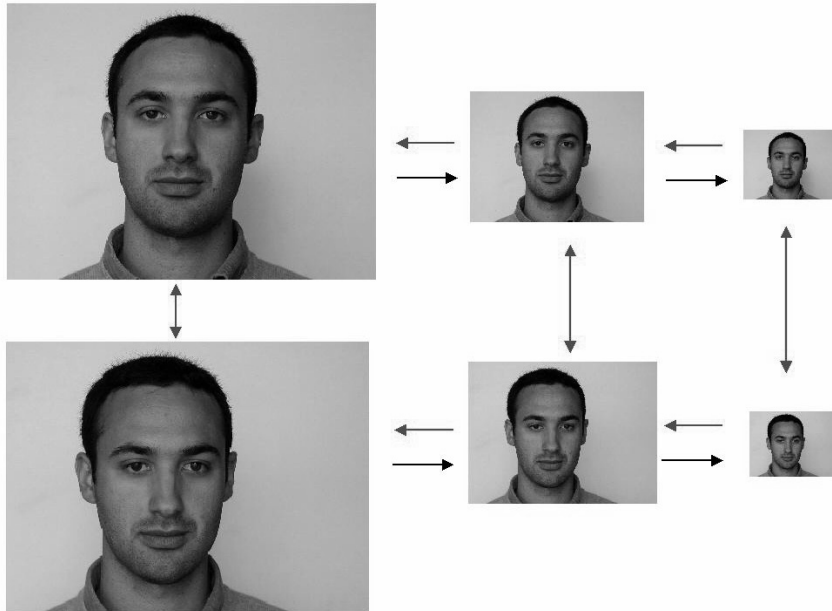In figure 8 we illustrate the pyramidal approach.

Π

Figure 8: Illustration of the pyramidal procedure to compute the disparity

2.4 Invariance Under Linear Grey-value Transformations

A remaining shortcoming of the modified model is that the energy functional is not invariant under grey level transformation of the form $(I, I') \rightarrow (kI, kI')$, where k is a constant. Therefore, the choice of the parameters depends strongly on the image contrast.

This problem can be solved as follows. We compute C and ν by specifying two parameters $\alpha, s \in (0, 1)$ such that

$$C = \frac{\alpha}{\max\limits_{(x,y)}(|(\nabla I_{\max})(x,y)|^2)},$$

$$s = \int_0^\nu \mathcal{H}_{|\nabla I_{\max}|}(z) dz$$

where $\mathcal{H}_{|\nabla I_{\max}|}(z)$ represents the normalized histogram of $|\nabla I_{\max}|$. We name s the *isotropy fraction*. When $s \rightarrow 0$, the diffusion operator becomes anisotropic at all locations, and when $s \rightarrow 1$, it leads to isotropic diffusion everywhere. In practical applications of our method it is thus sufficient to specify the parameters α and s instead of C and ν.

12

3   Existence and Uniqueness of the Parabolic Equation

To apply a gradient descent method to the Euler-Lagrange equation yields to solve the associated parabolic equation:

$$
\begin{aligned}
\frac{\partial \lambda}{\partial t} \;=\;& C \operatorname{div} \left(D \left(\nabla I_{\max} \right) \nabla \lambda \right) \\
& + \sum_{i=1}^{3} \left(I_i(\overrightarrow{x}) - I_i'(\overrightarrow{x}) \right) \frac{a \left(\frac{\partial I_i'}{\partial y} \right)^{\lambda} (\overrightarrow{x}) - b \left(\frac{\partial I_i'}{\partial x} \right)^{\lambda} (\overrightarrow{x})}{\sqrt{a^2 + b^2}},
\end{aligned}
\tag{8}
$$

the asymptotic state of this equation when $t \to \infty$ provides the disparity. This equation leads to a mathematically correct concept, we shall prove existence and uniqueness in the Appendix. We obtain the following result.

THEOREM: *If I, I' are enough regular functions, then, for any initial datum $\lambda^0 \in L^2(\mathbb{R}^2, \mathbb{R})$, there exists a unique solution of the above partial differential equation.*

It's worth to point out here that we will use the technique developed in [2] in order to proof the above theorem.

4   Numerical Analysis

In order to compute the disparity, we will use a finite difference discretization of the above partial differential equation. We note by $D(\nabla I_{\max})$ in a pixel (i, j) the matrix

$$
D(\nabla I_{\max})_{ij} = \begin{pmatrix} d_{ij} & e_{ij} \\ e_{ij} & f_{ij} \end{pmatrix}
$$

The numerical algorithm that we propose is based on the next implicit implementation of the partial differential equation (8):

$$\frac{\lambda_{i,j}^{k+1} - \lambda_{i,j}^k}{\tau} = C \left(\frac{d_{i+1,j} + d_{i,j}}{2} \frac{\lambda_{i+1,j}^{k+1} - \lambda_{i,j}^{k+1}}{h_1^2} + \frac{d_{i-1,j} + d_{i,j}}{2} \frac{\lambda_{i-1,j}^{k+1} - \lambda_{i,j}^{k+1}}{h_1^2} \right.$$

$$+ \frac{f_{i,j+1} + f_{i,j}}{2} \frac{\lambda_{i,j+1}^{k+1} - \lambda_{i,j}^{k+1}}{h_2^2} + \frac{f_{i,j-1} + f_{i,j}}{2} \frac{\lambda_{i,j-1}^{k+1} - \lambda_{i,j}^{k+1}}{h_2^2}$$

$$+ \frac{e_{i+1,j+1} + e_{i,j}}{2} \frac{\lambda_{i+1,j+1}^{k+1} - \lambda_{i,j}^{k+1}}{2h_1 h_2} + \frac{e_{i-1,j-1} + e_{i,j}}{2} \frac{\lambda_{i-1,j-1}^{k+1} - \lambda_{i,j}^{k+1}}{2h_1 h_2}$$

$$- \frac{e_{i+1,j-1} + e_{i,j}}{2} \frac{\lambda_{i+1,j-1}^{k+1} - \lambda_{i,j}^{k+1}}{2h_1 h_2} - \left. \frac{e_{i-1,j+1} + e_{i,j}}{2} \frac{\lambda_{i-1,j+1}^{k+1} - \lambda_{i,j}^{k+1}}{2h_1 h_2} \right)$$

$$+ \sum_{l=1}^{3} \left(I_l(\overrightarrow{x}_{i,j}) - I_l'^{\lambda_{i,j}^k}(\overrightarrow{x}_{i,j}) - \frac{\lambda_{i,j}^{k+1} - \lambda_{i,j}^k}{\sqrt{a_{i,j}^2 + b_{i,j}^2}} \left(a_{i,j} \left(\frac{\partial I_l'}{\partial x} \right)^{\lambda_{i,j}^k}(\overrightarrow{x}_{i,j}) - b_{i,j} \left(\frac{\partial I_l'}{\partial y} \right)^{\lambda_{i,j}^k}(\overrightarrow{x}_{i,j}) \right) \right)$$

$$\cdot \frac{a_{i,j} \left(\frac{\partial I_l'}{\partial x} \right)^{\lambda_{i,j}^k}(\overrightarrow{x}_{i,j}) - b_{i,j} \left(\frac{\partial I_l'}{\partial y} \right)^{\lambda_{i,j}^k}(\overrightarrow{x}_{i,j})}{\sqrt{a_{i,j}^2 + b_{i,j}^2}} \tag{9}$$

where τ is the time step size, h_1 and h_2 denote the pixel size in x and y direction, respectively, $\lambda_{i,j}^k$ approximates λ in some grid point $\overrightarrow{x}_{i,j}$ at time $k\tau$. We calculate values outside grid points by linear interpolation, and we solve the resulting linear system of equations iteratively by a symmetric Gauß–Seidel algorithm [4].

The linear implicit scheme offers the advantage of using large time steps in order to accelerate convergence to the steady state.

5 $3 - D$ Reconstruction and Experimental Results.

Our algorithm for computing the disparity depends on a number of parameters that have an intuitive meaning:

- The regularization parameter α specifies the balance between the smoothing term and the equality of the 3 color channels for the corresponding points. Larger values lead to smoother flow fields by filling the information from image edges.

- The isotropy fraction s determines the contrast parameter ν

- The number of times n_0 that we sample the image stereo pair in the pyramidal approach.

- The time step τ for solving the linear system to go from λ_{ij}^k to λ_{ij}^{k+1}, and the stopping time T for computing the asymptotic state of the parabolic equation. These are pure numerical parameters. We experiences that fixing $\tau = 4$ and $T = 500$ create results that are sufficiently close to the asymptotic state.

The first experience of 3-D geometry reconstruction that we present corresponds to the stereo pair given in figure 9 (at the end of the document). In this experience, the projection matrix P and P', and the fundamental matrix F, obtained using the calibration object of figure 4 are given by:

$$P = \begin{pmatrix} 1396 & -1308 & -15.54 & 1485116 \\ 201.7 & 189.2 & -1872 & 1687977 \\ 0.7846 & 0.6186 & 0.0394 & 4103 \end{pmatrix} \quad P' = \begin{pmatrix} 1501 & -1101 & 73.05 & 1468058 \\ 385.1 & 354.1 & -1764 & 1481735 \\ 0.69466 & 0.69548 & 0.18373 & 3953 \end{pmatrix}$$

$$F = \begin{pmatrix} 0.738724 & 0.841469 & -12056.94 \\ -0.46314623 & -0.645678 & 8582.56 \\ 11312.11 & -8491.66 & 594096.29 \end{pmatrix}$$

In figure 9, we present 4 views of the $3 - D$ reconstruction of the stereo pair using the disparity computed by the method proposed in this paper.

The second experience of 3-D geometry reconstruction that we present corresponds to the stereo pair given in figure 10. In this experience, the projection matrix P and P', and the fundamental matrix F, are the same that in the first experience.

We notice that the results are very accurate, we have to take into account that human faces are really difficult objects because the human vision is very sensitive to the human face shapes, so, in particular, we are very sensitive to the error in the $3 - D$ shape reconstruction.

Finally, In figure 11, we present a numerical experience based on 2 outdoor views of the *Instituto Universitario de Ciencias y Tecnologías Cibernéticas de la Universidad de Las Palmas de Gran Canaria*. In figure 11 we present the stereo pair as well as 4 views of the $3 - D$ geometry reconstruction using the method proposed in this paper. The results are fair but not so perfect as in the case of the human faces because, on the one hand, there are multiple occlusion phenomena in the scene, an on the other hand the textures of the ground and the wall are very homogeneous and then, to find out the correspondence between points is more difficult.

Concerning the choice of the parameters, we have taken $n_0 = 4$ and $\alpha = 1.5$ in all the experiences. We have taken $s = 0.5$ in the case of the human faces and $s = 0.2$ in the case of the outdoor scene, in order to keep better the strong discontinuities of the disparity

15

present in this scene. We notice that the algorithm is very robust with respect to the choice of the parameters and that with equal or similar values, we obtain good results in very different situations.

For more details about the numerical experiences you can visit the web site: http://serdis.dis.ulpgc.es/~lalvarez/research/demos/ColorStereoFlow.

References

[1] L. Alvarez, P.-L. Lions, J.-M. Morel, *Image selective smoothing and edge detection by nonlinear diffusion. II*, SIAM J. Numer. Anal., Vol. 29, 845–866, 1992.

[2] L. Alvarez, R.Deriche, J.Sánchez and J.Weickert, *Dense disparity map estimation respecting image discontinuities: A PDE and Scale-Space Based Approach*, INRIA Rapport de Recherche N°3874, 2000

[3] L. Alvarez, J. Weickert, J. Sánchez, *A scale-space approach to nonlocal optical flow calculations*, M. Nielsen, P. Johansen, O.F. Olsen, J. Weickert (Eds.), Scale-space theories in computer vision, Lecture Notes in Computer Science, Springer, Berlin, Vol. 1682, 235–246, 1999.

[4] L. Alvarez, J. Weickert, J. Sánchez, *Reliable Estimation of Optical Flow for Large Displacements*, Technical Report No. 2, Cuadernos del Instituto Universitario de Ciencias y Tecnologías Cibernéticas, Universidad de Las Palmas de Gran Canaria, Spain, 1999.

[5] N. Ayache and C. Hansen. Rectification of images for binocular and trinocular stereovision. In *Ninth International Conference on Pattern Recognition*, pages 11–16, October 1988, Beijing, China.

[6] N. Ayache and F. Lustman. Fast and reliable passive trinocular stereovision. In *Proceedings of the 1st International Conference on Computer Vision*, pages 422–427, London, England, June 1987. IEEE Computer Society Press.

[7] S.T. Barnard. Stochastic Stereo Matching Over Scale. *International Journal of Computer Vision*, Vol. 3, 17–32, 1989.

[8] J.L. Barron, D.J. Fleet, and S.S. Beauchemin. Performance of optical flow techniques. *International Journal of Computer Vision*, 12(1):43–77, 1994.

[9] B. Bascle and R. Deriche. Energy based methods for 2D curve tracking, reconstruction, and refinement of 3D curves and applications. In *SPIE Proceedings, Vol. 2031, B.C. Vemuri (Ed.), Geometric Methods in Computer Vision II*, San-Diego, California,USA, July 12-13, 1993, pages 282–293.

[10] F. Bergholm, *Edge focusing*, IEEE Trans. Pattern Anal. Mach. Intell., Vol. 9, 726–741, 1987.

[11] H. Brezis, *Opérateurs maximaux monotones et semi-groupes de contractions dans les espaces de Hilbert*, North Holland, Amsterdam, 1973.

[12] A.T. Brint and M. Brady. Stereo Matching of Curves. *Image and Vision Computing*, Vol. 8, No. 1, pp. 50–56, 1990.

[13] P. Charbonnier, L. Blanc–Féraud, G. Aubert, M. Barlaud,

   Two deterministic half-quadratic regularization algorithms for computed imaging, Proc. IEEE Int. Conf. Image Processing (ICIP–94, Austin, Nov. 13–16, 1994), Vol. 2, IEEE Computer Society Press, Los Alamitos, 168–172, 1994.

[14] R. Deriche and O. Faugeras. Les EDP en traitement des images et vision par ordinateur. *Traitement du Signal* Vol. 13, No. 6, 1996 (also as INRIA Research Report 2697, Nov. 1995).

[15] Frédéric Devernay and Olivier D. Faugeras. Computing differential properties of 3-D shapes from stereoscopic images without 3-D models. Proc. IEEE Conference on Computer Vision and Pattern Recognition, Seattle, WA, June 21–23, 1994, pages 208–213.

[16] W. Enkelmann, *Investigation of multigrid algorithms for the estimation of optical flow fields in image sequences*, Computer Vision, Graphics and Image Processing, Vol. 43, 150–177, 1988.

[17] O. Faugeras. *Three-Dimensional Computer Vision: a Geometric Viewpoint*. MIT Press, Cambridge, MA, 1993.

[18] Olivier Faugeras, Bernard Hotz, Hervé Mathieu, Thierry Viéville, Zhengyou Zhang, Pascal Fua, Eric Théron, Laurent Moll, Gérard Berry, Jean Vuillemin, Patrice Bertin, and Catherine Proy. Real time correlation based stereo: algorithm implementations and applications. *International Journal of Computer Vision*. To appear.

[19] D.J. Fleet and A.D. Jepson. Computation of component image velocity from local phase information. *International Journal of Computer Vision*, 5:77–104, 1990.

[20] D.J. Fleet and A.D. Jepson. Stability of phase information. *IEEE Trans. Patt. Anal. Mach. Intel.*, 15:1253–1268, 1993.

[21] L. Florack, *Image Structure*, Kluwer, Dordrecht, 1997.

[22] Pascal Fua. A parallel stereo algorithm that produces dense depth maps and preserves image features. *Machine Vision and Applications*, 6(1): 35–49, Winter 1993. Available as INRIA research report 1369.

[23] W.E.L. Grimson *Computational Experiments with a Feature Based Stereo Algorithm*, IEEE Trans. Pattern Anal. Mach. Intell., Vol 7, No 1, January 1985 17–34, 1985 (See also MIT Memo 762, January 1984).

[24] D. Geman, G. Reynolds, *Constrained restoration and the recovery of discontinuities*, IEEE Trans. Pattern Anal. Mach. Intell., 14, 367–383, 1992

[25] F. Heitz, P. Pérez, and P. Bouthemy. Multiscale minimization of global energy functions in some visual recovery problems. *CVGIP : Image Understanding*, 59(1):125–134, January 1994.

[26] T. Iijima, *Basic theory on normalization of pattern (in case of typical one-dimensional pattern)*, Bulletin of the Electrotechnical Laboratory, Vol. 26, 368–388, 1962 (in Japanese).

[27] M.R.M. Jenkin and A.D. Jepson. Recovering local surface structure through local phase difference methods. *CVGIP: Image Understanding*, 59:72–93, 1994.

[28] D.G. Jones, J. Malik, *A computational framework for determining stereo correspondence from a set of linear spatial filters*, G. Sandini (Ed.), Computer vision – ECCV '92, Lecture Notes in Computer Science, Vol. 588, Springer, Berlin, 395–410, 1992.

[29] J.J. Koenderink, *The structure of images*, Biological Cybernetics, Vol. 50, 363–370, 1984.

[30] T. Lindeberg, *A scale selection principle for estimating image deformations*, Image and Vision Computing, Vol. 16, No. 14, 961–977, 1998.

[31] J.H. McIntosh and K.M.Mutch. *Matching Straight Lines*, Computer Vision, Graphics and Image Processing, 43(3):386-29, 1998.

[32] G.Medioni and R.Nevatia *Segment Based Stereo Matching*, Computer Vision, Graphics and Image Processing, 31(1):2–18, 1985.

[33] K.W. Morton, L.M. Mayers, *Numerical Solution of Partial Differential Equations*, Cambridge University Press, Cambridge, 1994.

[34] H.-H. Nagel, *Constraints for the estimation of displacement vector fields from image sequences*, Proc. Eighth Int. Joint Conf. on Artificial Intelligence (IJCAI '83, Karlsruhe, August 8–12, 1983), 945–951, 1983.

[35] H.-H. Nagel, *On the estimation of optical flow: relations between different approaches and some new results*, Artificial Intelligence, Vol. 33, 299–324, 1987.

[36] H.-H. Nagel, W. Enkelmann, *An investigation of smoothness constraints for the estimation of displacement vector fields from images sequences*, IEEE Trans. Pattern Anal. Mach. Intell., Vol. 8, 565–593, 1986.

[37] M. Nielsen, R. Deriche, Binocular dense depth reconstruction using isotropy constraint, G. Borgefors (Ed.), Theory and applications of image processing II – selected articles from the 9th Scandinavian Conference on Image Analysis, World Scientific Publishing, Singapore, 27–140, 1995.

[38] M. Nielsen, R. Maas, W.J. Niessen, L.M.J. Florack, B.M. ter Haar Romeny, *Binocular stereo from grey-scale images*, J. Math. Imag. Vision, Vol. 10, 103–122, 1999.

[39] N.M.Nasrabadi. A Stereo Vision Technique Using Curve-Segments and Relaxation Matching, *IEEE Trans. Pattern Anal. Mach. Intell.*, 14(5), 566-572, May, 1992

[40] Keith Nishihara. Practical real-time imaging stereo matcher. *Optical Engineering*, 23(5), 536–545, 1984. See also MIT AI MEMO-772, August 1984.

[41] Y. Ohta and T. Kanade. Stereo by intra- and inter-scanline search. *IEEE Transactions on Pattern Analysis and Machine Intelligence*, 7:139–154, 1985.

[42] P. Perona, J. Malik, *Scale space and edge detection using anisotropic diffusion*, IEEE Trans. Pattern Anal. Mach. Intell., Vol. 12, 629–639, 1990.

[43] S.B. Pollard, J.E.W. Mayhew, and J.P. Frisby. PMF : a stereo correspondence algorithm using a disparity gradient constraint. *Perception*, 14:449–470, 1985.

[44] M. Pollefeys, R. Koch, and L. Van Gool. A simple and efficient rectification method for general motion. In *Proceedings of the 7th International Conference on Computer Vision*, pages 496–501, Corfu, Greece, Sept. 21–24, 1999. IEEE Computer Society Press.

[45] M. Proesmans, E. Pauwels, L. Van Gool, *Coupled geometry-driven diffusion equations for low-level vision*, B.M. ter Haar Romeny (Ed.), Geometry-driven diffusion in computer vision, Kluwer, Dordrecht, 191–228, 1994.

[46] L. Robert, R. Deriche, *Dense depth map reconstruction: A minimization and regularization approach which preserves discontinuities*, B. Buxton, R. Cipolla (Eds.), Computer vision – ECCV '96, Volume I, Lecture Notes in Computer Science, Vol. 1064, Springer, Berlin, 439–451, 1996.

[47] Luc Robert and Olivier Faugeras. Curve-based stereo: Figural continuity and curvature. In *Proceedings of the International Conference on Computer Vision and Pattern Recognition*, pages 57–62, Lahaina, Hawai, June 3–6, 1991. IEEE Computer Society Press.

[48] L.I. Rudin, S. Osher, E. Fatemi, *Nonlinear total variation based noise removal algorithms*, Physica D, Vol. 60, 259–268, 1992.

[49] J. Shah, *A nonlinear diffusion model for discontinuous disparity and half-occlusions in stereo*, Proc. IEEE Comp. Soc. Conf. Computer Vision and Pattern Recognition (CVPR '93, New York, June 15–17, 1993), IEEE Computer Society Press, Los Alamitos, 34–40, 1993.

[50] M.A. Snyder, *On the mathematical foundations of smoothness constraints for the determination of optical flow and for surface reconstruction*, IEEE Trans. Pattern Anal. Mach. Intell., Vol. 13, 1105–1114, 1991.

[51] J. Sporring, M. Nielsen, L. Florack, P. Johansen (Eds.), *Gaussian Scale-Space Theory*, Kluwer, Dordrecht, 1997.

[52] A.N. Tikhonov, V.Y. Arsenin, *Solutions of Ill–Posed Problems*, John Wiley & Sons, Washington, D.C., 1977.

[53] J. Weickert, *Theoretical foundations of anisotropic diffusion in image processing*, Computing, Suppl. 11, 221–236, 1996.

[54] J. Weickert, *Anisotropic Diffusion in Image Processing*, Teubner, Stuttgart, 1998.

[55] J. Weickert, S. Ishikawa, A. Imiya, *Linear scale-space has first been proposed in Japan*, J. Math. Imag. Vision, Vol. 10, 237–252, 1999.

[56] N. Yokoya. Stereo Surface Reconstruction by Multiscale-Multistage Regularization. Technical Report TR-90-45, ETL Electrotechnical Laboratory, Tsukuba, Japan, November 1990.

[57] Cyril Zeller and Olivier Faugeras. Applications of non-metric vision to some visually guided tasks. In *Proceedings of the International Conference on Pattern Recognition*, pages 132–136, Jerusalem, Israel, October 1994. Computer Society Press. Longer version available as INRIA Research Report RR2308.

6 Appendix. Existence and Uniqueness of the Parabolic Equation

We show the existence and uniqueness of solution of the parabolic equation (8) The parameters C and ν can be arbitrary positive real numbers. First we introduce an abstract

framework where we study the above system. This framework is used to show the existence and uniqueness of the solutions afterwards.

Abstract Framework

For simplicity, we will assume that the images are defined in $\mathbb{R}^2$. We define $H := L^2(\mathbb{R}^2, \mathbb{R})$, and the differential operator $A : D(A) \subset H \to H$ given by:

$$A(\lambda) = -C\mathrm{div}\left(D\left(\nabla I_{\max}\right)\nabla\lambda\right).$$

we define $\Omega = \mathbb{R}^2 \times \mathbb{R}^2 \times \mathbb{R}^2$. We will assume that $I, I' \in W^{1,\infty}(\mathbb{R}^2, \Omega)$. Therefore $\nabla I_{\max}$ is bounded and the eigenvalues of matrix $D\left(\nabla I_{\max}\right)$ are strictly positive. Therefore, as $C > 0$, the operator $A(\lambda)$ is a maximal monotone operator. For more details about maximal monotone operators we refer to Brezis [11]. Next, let us introduce the function $F : H \to H$ defined by

$$F(\lambda) = \sum_{i=1}^{3}\left(I_i - I'_i(Id + \overrightarrow{h}(\lambda))\right)\frac{-a\frac{\partial I'_i}{\partial y}(Id + \overrightarrow{h}(\lambda)) + b\frac{\partial I'_i}{\partial x}(Id + \overrightarrow{h}(\lambda))}{\sqrt{a^2 + b^2}}$$

Then the abstract evolution problem can be written as

$$\begin{cases} \frac{\partial \lambda}{\partial t} + A(\lambda) = F(\lambda) \in H & \forall t \in [0, T] \\ \lambda(0) = \lambda^0 \in H. \end{cases} \tag{10}$$

Any classical solution $\lambda \in C^1([0, T]; H) \cap C([0, T]; D(A))$ of (10) is given by:

$$\lambda(t) = S(t)\lambda^0 + \int_0^t S(t - s)F(\lambda(s))\,ds, \tag{11}$$

where $\{S(t)\}_{t>0}$ is the contraction semi-group that is associated to the homogeneous problem.

Definition. *We say that $h \in C([0, T]; H)$ is a generalized solution of (10) if it satisfies (11).*

Existence and Uniqueness Result

To simplify the discussion, we will assume that the epipolar line satisfies that $a^2 + b^2$ is strictly positive. In fact, the case $a = b = 0$ corresponds to epipolar lines located at the infinity plane ($m_3 = 0$), which is of course not very interesting from a practical point of view. In order to prove existence and uniqueness, we have to establish a lemma first.

Lemma. *Let us assume that $I, I' \in W^{1,\infty}(\mathbb{R}^2, \Omega)$, then F is a Lipschitz function.*

Proof: Given $\lambda_1, \lambda_2 \in H$, we have the following pointwise estimate

$$|F(\lambda_1) - F_i(\lambda_2)| =$$

$$\left| \sum_{i=1}^{3} (I_i - I_i'(Id + \overrightarrow{h}(\lambda_1))) \left(\frac{-b\frac{\partial I\prime_i}{\partial x}(Id + \overrightarrow{h}(\lambda_1))}{\sqrt{a^2 + b^2}} + \frac{a\frac{\partial I\prime_i}{\partial y}(Id + \overrightarrow{h}(\lambda_1))}{\sqrt{a^2 + b^2}} \right) \right.$$

$$\left. - (I_i - I_i'(Id + \overrightarrow{h}(\lambda_2))) \left(\frac{-b\frac{\partial I\prime_i}{\partial x}(Id + \overrightarrow{h}(\lambda_2))}{\sqrt{a^2 + b^2}} + \frac{a\frac{\partial I\prime_i}{\partial y}(Id + \overrightarrow{h}(\lambda_2))}{\sqrt{a^2 + b^2}} \right) \right|,$$

$$\leq \sum_{i=1}^{3} |I_i(Id + \overrightarrow{h}(\lambda_1))\partial_j I_i'(Id + \overrightarrow{h}(\lambda_1)) - I_i(Id + \overrightarrow{h}(\lambda_2))\partial_j I_i'(Id + \overrightarrow{h}(\lambda_2))|$$

$$+ |I_i| . |\partial_j I\prime_i(Id + \overrightarrow{h}(\lambda_1)) - \partial_j I\prime_i(Id + \overrightarrow{h}(\lambda_2))|,$$

$$\leq \sum_{i=1}^{3} \frac{1}{2} \left| \frac{-b\frac{\partial(|I_i'|^2)}{\partial x}(Id + \overrightarrow{h}(\lambda_1))}{\sqrt{a^2 + b^2}} - \frac{-b\frac{\partial(|I_i'|^2)}{\partial x}(Id + \overrightarrow{h}(\lambda_2))}{\sqrt{a^2 + b^2}} \right|$$

$$+ \frac{1}{2} \left| \frac{a\frac{\partial(|I_i|^2)}{\partial y}(Id + \overrightarrow{h}(\lambda_1))}{\sqrt{a^2 + b^2}} - \frac{a\frac{\partial(|I_i'|^2)}{\partial y}(Id + \overrightarrow{h}(\lambda_2))}{\sqrt{a^2 + b^2}} \right|$$

$$+ \|I\|_\infty \cdot \left| \frac{-b\frac{\partial I_i'}{\partial x}(Id + \overrightarrow{h}(\lambda_1))}{\sqrt{a^2 + b^2}} - \frac{-b\frac{\partial I\prime_i}{\partial x}(Id + \overrightarrow{h}(\lambda_2))}{\sqrt{a^2 + b^2}} \right|$$

$$+ \|I\|_\infty \cdot \left| \frac{a\frac{\partial I\prime_i}{\partial y}(Id + \overrightarrow{h}(\lambda_1))}{\sqrt{a^2 + b^2}} - \frac{a\frac{\partial I_i'}{\partial y}(Id + \overrightarrow{h}(\lambda_2))}{\sqrt{a^2 + b^2}} \right|,$$

$$\leq \sum_{i=1}^{3} \left\| |I_i'|^2 \right\|_{W^{1,\infty}} . |\overrightarrow{h}(\lambda_1) - \overrightarrow{h}(\lambda_2)| + 2\|I\|_\infty . \|I_i'\|_{W^{1,\infty}} . |\overrightarrow{h}(\lambda_1) - \overrightarrow{h}(\lambda_2)|$$

$$\leq \sum_{i=1}^{3} \left(\left\| |I_i'|^2 \right\|_{W^{1,\infty}} + 2\|I\|_\infty . \|I_i'\|_{W^{1,\infty}} \right) |\lambda_1 - \lambda_2|,$$

We conclude the proof of the lemma by setting

$$L = \sum_{i=1}^{3} \left(\left\| |I_i'|^2 \right\|_{W^{1,\infty}} + 2\|I\|_\infty . \|I_i'\|_{W^{1,\infty}} \right) .$$

This shows the assertion of the lemma.

Now we can prove the existence and uniqueness theorem

THEOREM: *If $I, I' \in W^{1,\infty}(\mathbb{R}^2, \Omega)$ then for any initial datum $\lambda^0 \in L^2(\mathbb{R}^2)$, there exists a unique solution of (8).*

Proof: Using the previous lemma we deduce that F is lipschitz. Assume that $\lambda_1(t)$ and $\lambda_2(t)$ are solutions of (11) for initial conditions $\lambda_1(0)$ and $\lambda_2(0)$, then we have, using the fact that $-A$ is dissipative (which yields $\|S(t)f\|_H \leq \|f\|_H$), and the Lipschitz continuity of F the following estimate.

$$\|\lambda_1(t) - \lambda_2(t)\|_H \leq \|\lambda_1(0) - \lambda_2(0)\|_H + L \int_0^t \|\lambda_1(s) - \lambda_2(s)\|_H ds.$$

Applying the Gronwall–Bellman lemma [11] gives

$$\|\lambda_1(t) - \lambda_2(t)\|_H \leq e^{Lt}.\|\lambda_1(0) - \lambda_2(0)\|_H,$$

which yields uniqueness of the solution if it exists. Now consider the Banach space defined by

$$E = \{\lambda \in C\left([0, \infty); H\right) \ such \ that \ \sup_{t \geq 0} \|\lambda(t)\|_H e^{-Kt} < \infty\}$$

endowed with the norm $\|\lambda\|_E = \sup_{t \geq 0} \|\lambda(t)\|_H e^{-Kt}$. Let $\phi : E \to C\left([0, \infty); H\right)$ be defined by

$$\phi(\lambda)(t) = S(t)d^0 + \int_0^t S(t - s)F(\lambda(s))\, ds.$$

If $K > L$, then $\phi(E) \subset E$, and ϕ is $\frac{L}{K}$-Lipschitz since

$$\|\phi(\lambda_1) - \phi(\lambda_2)\|_E = \sup_{t \geq 0} \|\phi(\lambda_1)(t) - \phi(\lambda_2)(t)\|_H e^{-Kt},$$

$$\leq \sup_{t \geq 0} \int_0^t L\|\lambda_1(s) - \lambda_2(s)\|_H\, ds\, e^{-Kt}$$

$$\leq \sup_{t \geq 0} L\|\lambda_1 - \lambda_2\|_E.e^{-Kt} \int_0^t e^{Ks} ds$$

$$\leq \sup_{t \geq 0} \frac{L}{K}\|\lambda_1 - \lambda_2\|_E.e^{-Kt}(e^{Kt} - 1)$$

$$\leq \frac{L}{K}\|\lambda_1 - \lambda_2\|_E.$$

We deduce that ϕ is a contraction, and by Banach's fixed point theorem there exists a unique λ such that $\phi(\lambda) = \lambda$. This is the generalized solution of (10), and the proof is concluded.
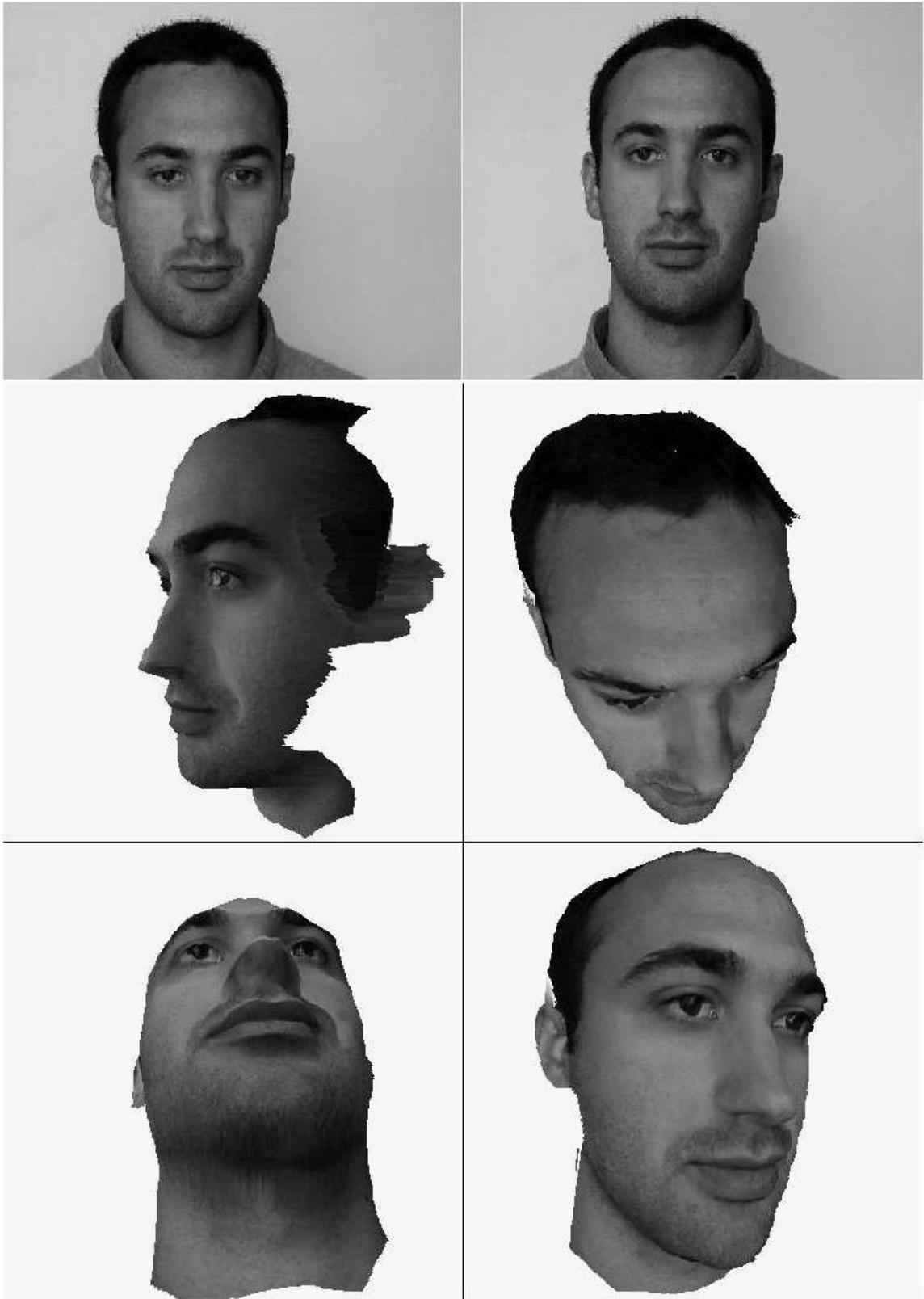
Figure 9:

Figure 10:

Figure 11: